Available online at www.sciencedirect.com
SCIENCE DIRECT®
Polymer 45 (2004) 1383–1389
polymer
www.elsevier.com/locate/polymer

Brownian dynamics simulations of bead-rod-chain in simple shear flow and elongational flow

S. Liu, B. Ashok, M. Muthukumar*

Department of Physics and Polymer Science and Engineering, University of Massachusetts, Amherst, MA 01003, USA

Received 20 March 2003; received in revised form 2 July 2003; accepted 5 July 2003

Abstract

We have simulated a dilute polymer solution under simple shear and elongational flows using the bead-rod-chain model, by incorporating intra-chain hydrodynamic interaction and excluded volume effects. Configurational properties and rheological quantities were calculated. For the simple shear flow, shear rate dependencies of chain's size, shape, and rotation were monitored. Shear-thinning was observed at all shear rates. In addition, the critical strain rate, ε_c, at which the polymer undergoes a coil-stretch transition under elongational flow, was investigated. The slope at the inflection point of the $\log(R_g^2)$ vs $\log(\varepsilon)$ curve increased as the chain length increased, indicating a possible first order transition, in agreement with theories and experiments.

Keywords: Shear-thinning; Shear-thickening; Brownian dynamics simulation

1. Introduction

Polymer liquids in flows exhibit several interesting phenomena. Such behavior is typically due to the non-Newtonian nature of the macromolecular fluid. For example, polymer solutions and melts in shear flows undergo a decrease in viscosity with increase in shear rate. This shear-thinning behavior is observed in most polymer solutions that have a shear rate dependent viscosity, although there are a few polymer solutions that are dilatant (i.e. that exhibit shear-thickening). The normal stresses are also non-zero and shear rate dependent. There are many experimental investigations of shear-thinning (see, for example, [1–4]).

Another interesting phenomenon is the existence of the coil-stretch transition when the polymeric liquid is under an elongational flow. The nature of this transition is still unclear, although De Gennes has predicted the presence of a first order phase transition for two-dimensional elongational flows [5].

Experiments performed by Odell et al. and by others have shown the critical strain rate ε_c to be related to the molecular weight of the polymer by a power law, $\varepsilon_c \sim N^{-\beta}$, $\beta = 1.5$ independent of solvent quality [6–11]. Different values of β have also been reported by other authors for good solvents [12,13].

To calculate the rheological properties of the complex fluid, the exact approach would be to include the effect of solvent molecules as well as macromolecules. Although such calculations are extant, the overwhelming computational burdens involved make their application still very limited.

The solvent is therefore usually neglected and the system is approximated by theoretical models. The simplest model is the Rouse model [18], where the solvent is approximated by pure random noises. However, as it completely ignores the effect of excluded-volume and hydrodynamic interactions (HI), a simulation of a dilute polymer solution based on the Rouse model would not take into account the long-ranged hydrodynamic coupling, and would not predict shear-thinning behavior, nor yield correct scaling laws for material and transport functions.

The Kirkwood–Riseman–Zimm model [19,20] takes HI into account with a pre-averaging approximation and obtains correct scaling laws, but the material functions are independent of shear rate. Several authors have contributed other models, improving over the pre-averaging HI approximation and including excluded volume effects [21–28,35,37–40]. In particular, Fixman made a correction

* Corresponding author.
E-mail address: muthu@polysci.umass.edu (M. Muthukumar).

0032-3861/$ - see front matter © 2003 Published by Elsevier Ltd.
doi:10.1016/j.polymer.2003.07.012

to the Zimm pre-averaging approximation by his perturbative calculation of the effect of HI [21–25]. Öttinger developed a consistently averaging model and obtained the correct flow-rate dependence for the material functions [36]. Further details of theory, simulation models and experimental data, can be found in, for example, Bird et al. [31,32], Yamakawa [33], Öttinger [34] and in Petera and Muthukumar [38] (here-after referred to as P–M) and the references cited therein. Öttinger has explicitly reformulated the diffusion equation for polymer chains under constraints and with HI into a set of stochastic differential equations; he has demonstrated the construction of Brownian dynamics simulation algorithms and the technique of calculation therein of stresses [35]. P–M implemented Öttinger's bead-rod-chain model in a Brownian dynamics simulation with excluded volume effects and obtained correct shear-thinning behavior [38]. Here in this paper, following the same algorithm as in P–M, we have simulated a single freely jointed chain, with number of units N up to 60, under shear and elongational flows. We calculated both configurational and rheological quantities mainly in the mid and high strain rate regimes. We also paid attention to the coil-stretch transition in the low flow rate regime. As mentioned earlier, it is still debatable whether the coil-stretch transition is a first order transition; our simulations for short chains indicate that the transition approaches discontinuity as the chain length increases.

This paper proceeds as follows. We present our simulation model in some detail in Section 2. Section 3 gives the results of our simulations, and Section 4 contains the discussion of results and conclusions.

2. Algorithm

We modeled the polymer with $N+1$ beads connected by N freely rotating rigid rods of length l. The system is described by a diffusion equation derived by P–M from the work of Öttinger by using connector vectors instead of positional vectors.

If $\mathbf{R}_i$ denotes the position vector of the ith bead, the connector vector between beads i and $i-1$ will be given by $\mathbf{u}_i = \mathbf{R}_i - \mathbf{R}_{i-1}$. The stochastic differential equation for the connector vectors is [38]

$$
\begin{aligned}
\mathrm{d}\mathbf{u}_a = {} & \sum_b \mathbf{K}_{ab}\left(\left(\frac{1}{\zeta}\sum_{ci}\mathscr{H}_{bc}\tilde{B}_{ic}\mathbf{F}_i + \frac{kT}{\zeta}\sum_{cd}\mathscr{H}_{bc}N^0_{cd}C_{dc}\mathbf{u}_c + \boldsymbol{\Gamma}\mathbf{u}_b\right)\mathrm{d}t + \sqrt{\frac{2kT}{\zeta}}\sum_{ij}B_{bi}\mathbf{W}_{ij}\mathrm{d}\boldsymbol{\xi}_j\right) \\
& - \frac{kT}{\zeta}\sum_{bcd}\mathbf{K}_{ab}\left(\mathscr{H}_{bc}\mathscr{H}_{cd}\mathbf{u}_d N_{cd} + \sum_e \frac{\partial\mathscr{H}_{bc\alpha\beta}}{\partial\mathbf{u}_{d\delta}}\mathbf{u}_{c\gamma}\mathscr{H}_{de\delta\epsilon}\mathbf{u}_{e\epsilon}N_c e\right)\mathrm{d}t \\
& + \frac{kT}{\zeta}\sum_{bc}\mathscr{H}_{ab}\mathbf{u}_b N_{bc}\left(\mathbf{u}_d\mathscr{H}_{dc}\mathscr{H}_{ce}\mathbf{u}_e N_{de} - Tr\mathscr{H}_{cc}\right)\mathrm{d}t,
\end{aligned} \tag{1}
$$

where the indices $a, b, \ldots$, run from 1 to N and indices $i, j, \ldots$, from 0 to N.

In the above expression, ζ is the friction coefficient defined by using Stokes' law $\zeta = 6\pi\eta R_{\mathrm{hyd}}$, with each bead having the hydrodynamic radius R_{hyd}. The tensors B_{ij} and $\tilde{B}_{ij}$ transform between connector vectors and bead position vectors. $\mathscr{H}_{ab}$ is defined by $\mathscr{H}_{ab} = \sum_{ij} B_{ai}B_{bj}\mathbf{H}_{ij}$, with the hydrodynamic interaction tensor H_{ij} having the Cholesky decomposition $\mathbf{H}_{ij} = \sum_k \mathbf{W}_{ik}\mathbf{W}^{\mathrm{T}}_{jk}$. $\mathbf{W}_{ik}$ is the Cholesky decomposition of $\mathbf{H}_{ij}$. $\mathscr{W}_{ij}$, in turn, represents the Cholesky decomposition of $\mathscr{H}_{ij}$ and is used below.

For shear flows, Γ is the systematic shear flow matrix, $\dot{\gamma}\mathbf{e}_1\mathbf{e}_2^{\mathrm{T}}$, $\dot{\gamma}$ being the flow rate and $\mathbf{e}_i$ the unit vector in the ith direction. For elongational flows, Γ would represent, instead, the elongational flow matrix $\varepsilon(\mathbf{e}_1\mathbf{e}_1^{\mathrm{T}} - \frac{1}{2}\mathbf{e}_2\mathbf{e}_2^{\mathrm{T}} - \frac{1}{2}\mathbf{e}_3\mathbf{e}_3^{\mathrm{T}})$. $C_{ab} = \sum_i B_{ai}B_{bi}$ is the usual Kramers matrix, $M^0_{ab} = C_{ab}\mathbf{u}_a^{\mathrm{T}}\mathbf{u}_b$, $N^0_{ab} = ((M^0)^{-1})_{ab}$, $M_{ab} = \mathbf{u}_a\mathscr{H}_{ab}\mathbf{u}_b$, $N_{ab} = (M^{-1})_{ab}$ and $\mathbf{K}_{ab} = \delta_{ab} + N_{cb}\mathscr{H}_{ac}\mathbf{u}_c\mathbf{u}_b^{\mathrm{T}}$. $\mathbf{F}_i$ are the forces acting on bead i. A purely repulsive excluded volume is used. $\boldsymbol{\xi}_i$ is the random noise on bead i, satisfying

$$
\langle\boldsymbol{\xi}_i(t)\rangle = 0, \qquad \langle\boldsymbol{\xi}_i(t)\boldsymbol{\xi}_j^{\mathrm{T}}(t')\rangle = \delta_{ij}\mathbf{1}\delta(t-t'). \tag{2}
$$

The procedure used to solve the equation was as follows. The beads were first moved without any constraints

$$
\begin{aligned}
\mathbf{u}_a^{\mathrm{temp}} = {} & \mathbf{u}_a + \Big(\frac{1}{l\zeta}\sum_{ci}\mathscr{H}_{bc}\tilde{B}_{ic}\mathbf{F}_i + \frac{kT}{l^2\zeta}\sum_{cd}\mathscr{H}_{bc}N^0_{cd}C_{dc}\mathbf{u}_c \\
& + \boldsymbol{\Gamma}\mathbf{u}_b\Big)\Delta t + \sqrt{\frac{2kT\Delta t}{l^2\zeta}}\mathscr{W}_{ab}\Delta\boldsymbol{\xi}_b.
\end{aligned} \tag{3}
$$

The discrete noise is Gaussian

$$
\langle\Delta\boldsymbol{\xi}_i\rangle = 0, \qquad \langle\Delta\boldsymbol{\xi}_i\Delta\boldsymbol{\xi}_j^{\mathrm{T}}\rangle = \delta_{ij}\mathbf{1}. \tag{4}
$$

Constraints were then imposed by addition of forces containing Lagrange parameters σ_a

$$
\mathbf{u}_a^{\mathrm{new}} = \mathbf{u}_a^{\mathrm{temp}} - \sum_b \mathscr{H}'_{ab}\mathbf{u}_b^{av}\sigma_a \tag{5}
$$

with

$$
(\mathbf{u}_a^{\mathrm{new}})^2 = 1 \tag{6}
$$

$\mathscr{H}'_{ab}$ being evaluated at

$$
\mathbf{u}_b^{av} = \tfrac{1}{2}(\mathbf{u}_a + \mathbf{u}_a^{\mathrm{temp}}). \tag{7}
$$

Dimensionless variables are used in the simulation; $\overline{\Delta t} = kT\,\Delta t/l^2\zeta$, for the time step, $\bar{\gamma} = \dot{\gamma}l^2\zeta/kT$, the shear strength, $\bar{R}_{\mathrm{hyd}} = R_{\mathrm{hyd}}/l$, the radius of beads for hydrodynamic interaction, $\bar{R}_{\mathrm{ex}} = R_{\mathrm{ex}}/l$, radius of beads for the excluded volume interaction, and $\bar{A} = A/kT$, the strength of the excluded volume interaction. For further details on the equations used and the basis of their derivation, readers are referred to P–M [38] and the references therein.

The shear flow used was defined by the flow field **V** given by

$$V_x = \dot{\gamma}y \qquad V_y = V_z = 0. \tag{8}$$

The elongational flow employed was given by

$$V_x = \dot{\gamma}x \qquad V_y = -\tfrac{1}{2}\dot{\gamma}y \qquad V_z = -\tfrac{1}{2}\dot{\gamma}z. \tag{9}$$

The simulation protocols for both shear and elongational flow were as follows. An excluded volume chain was generated randomly in the solution. Then the Brownian dynamics calculations were performed with applied shear or elongational flow field. After a sufficiently long time (ranging from 10^5 to 10^7 BD time steps depending on the flow rate and chain length), to allow the system to reach a steady state, the co-ordinates of the connector vectors of the polymer were saved for every 1000 Brownian steps. The time step for a given simulation varied from 0.001 to 0.00001, depending on the magnitude of the flow field. The total simulation time varied from 10^6 steps to 5×10^7 steps.

For simulations with hydrodynamics, the computational time scales in proportion to N^3, N being the degree of polymerization. In P–M, a chain of up to $N = 20$ beads was simulated. By implementing a parallel algorithm we managed to simulate a chain of up to $N = 60$ beads. The simulations were carried out on a 24-node alpha Linux (533 MHZ) cluster. The typical run time for one simulation was around two weeks.

3. Results for shear flow

In order to verify our implementation of the algorithm described above, we simulated the same system as in P–M, but with a much longer chain, $N = 60$. A very good agreement was found on comparing the results of our long chain simulation to their simulation with shorter chains. Results are summarized in Sections 3.1 and 3.2.

3.1. Configurational quantities

We calculated the gyration tensor and radius of gyration of the polymer. The gyration tensor is defined by

$$\mathbf{G} = \frac{1}{2N^2}\sum_{i,j=0}^{N}\langle(\mathbf{R}_i - \mathbf{R}_j)(\mathbf{R}_i - \mathbf{R}_j)^{\mathrm{T}}\rangle. \tag{10}$$

The radius of gyration is obtained from

$$R_{\mathrm{g}}^2 = G_{xx} + G_{yy} + G_{zz}. \tag{11}$$

Diagonalization of **G** gives us its principal axes, D_{11}, D_{22} and D_{33}. D_{11} being in the direction of the flow, we would expect it to increase with increase in the shear rate, while the other two principal axes decrease in magnitude. The results are shown in Fig. 1 as functions of the reduced shear strength. Our plots are very similar to the corresponding figures shown in P–M. As expected, D_{11} increased as the shear rate increased, while both D_{22} and D_{33} decreased. The decrease of D_{33} is in contradiction with experimental results [14], where it is observed to be a constant, but it was noticed that D_{22} did, indeed, decrease at a much faster rate than D_{33}. The fact that D_{33} continued to decrease may be attributed to the fact that our model chain has a maximal extension and to the short chain effect, as was also pointed out by P–M.

The orientation angle θ, the angle of rotation of the principal axis with respect to the direction of shear flow, is defined as $\cot(2\theta) = \mathbf{G}_{xx} - \mathbf{G}_{yy}/2\mathbf{G}_{xy}$. Plots of θ as a function of the shear rate $\dot{\gamma}$ are shown in Fig. 2, for two different chain lengths ($N = 20$ and 60). As one would expect, the values of the orientation angle are smaller for the longer ($N = 60$) chain.

The rotational motion of the polymer around its center of mass when in a shear flow is expected and has been known in the literature. However, the exact mechanism of this rotation has been somewhat unclear, although in a recent work Aust et al. have looked into the rotation and deformation of small chains [42]. If a rod were placed in a shear-flow, it would just rotate about its center of mass. But the behavior of a polymer, a flexible chain, is not as obvious. A visualization of our simulation, as in Fig. 3, enables us to actually observe the polymer chain's periodic motion and come to definite conclusions. The five snap-shots were taken within one rotation cycle and are shown in sequence, in the order of increasing time, from top (Fig. 3(a)) to bottom

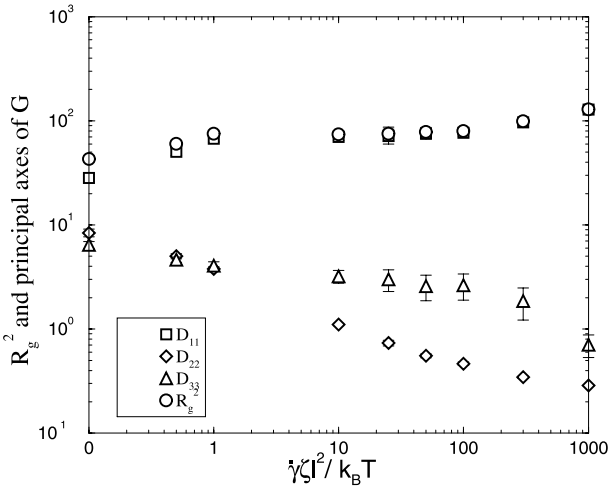

Fig. 1. Principal components of the gyration tensor and R_{g} versus shear rate.

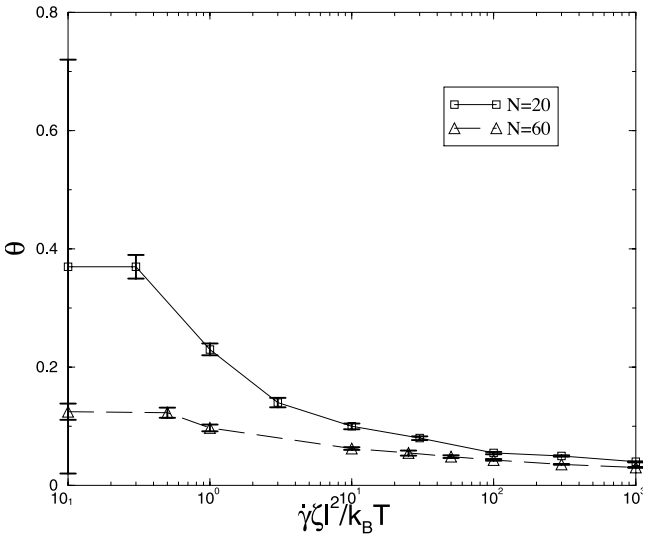

Fig. 2. Orientation angle of the chain versus dimensionless shear rate.

(Fig. 3(e)). The arrows in the figure show the direction of motion of the polymer segments relative to the center of mass.

The plot of Fig. 4 shows a graphical exposition of this behavior. It shows the position (projection on the x axis) of beads in a shear flow with $\dot{\gamma} = 10$, as a function of time. Beads 10 and 50 are located symmetrically at either end of the chain. As the chain stretches out and pulls back in again, periodically with time, in the shear flow, the positions of the beads accordingly oscillate about the center of mass (located at the origin).

It was found that at mid and high shear rates, the polymer rotated in a very distinct way: as it rotated, the rotation is

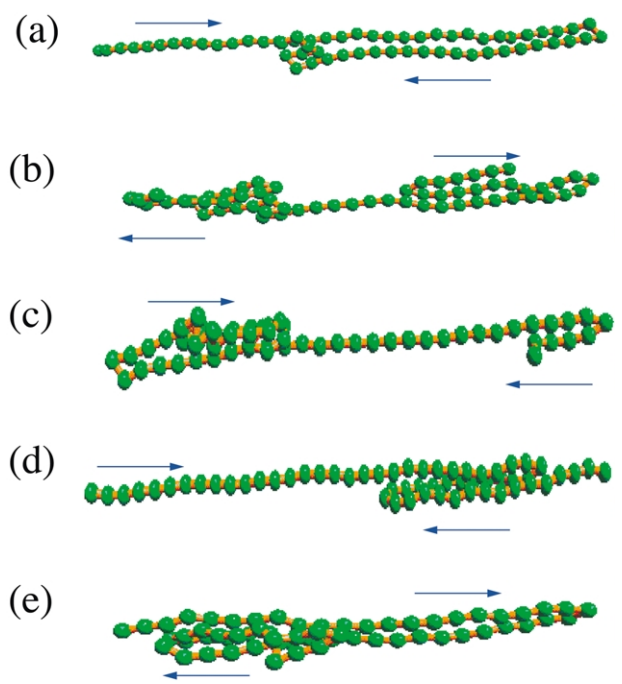

Fig. 3. Snap shots of the rotational motion of the polymer under shear flow with $\dot{\gamma} = 100$. Figures (a)–(e) are in the order of increasing time within the same rotational cycle.

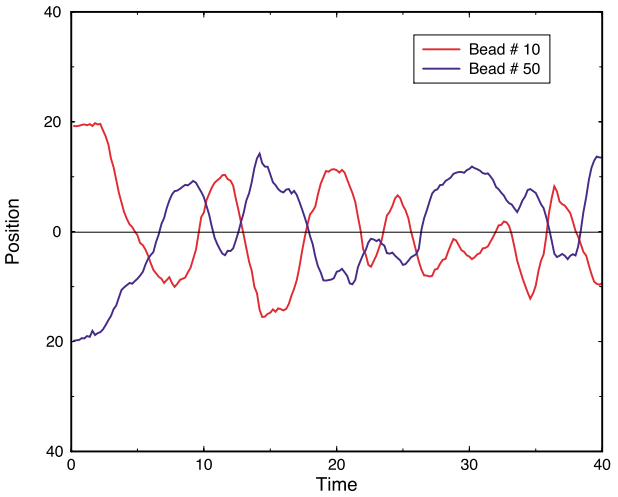

Fig. 4. Plot of position (projection on x-axis) of beads (numbers 10 and 50) in a shear flow (with shear rate $\dot{\gamma} = 10$) as a function of time.

confined to a plane with a fixed orientation angle, while its two hair-pins went backward and forward around the center of mass. Since the rotational component of the shear flow is proportional to the shear rate, $\dot{\gamma}$, we would expect the period of rotation to linearly depends on $\dot{\gamma}$. Fig. 5 shows the period of the rotational motion plotted vs the shear rate for our simulation. It can be seen that in the mid and high shear rate regime, the period is indeed linearly related to the shear rate. This dependence is, however, unclear for small shear rates, due to the large error bars for the simulation data in this regime (as seen in Fig. 2). The reason for the large value of error bars as shear rate tends to zero in Fig. 2, is that at low shear rates, the chain tends to have a spherical configuration. Therefore, the accuracy of the calculation of the preferred orientation is poor in that regime. Also, the model used for our simulations is not suitable for the polymer in the quiescent state, and we would have to reformulate the problem in order to accurately calculate material functions

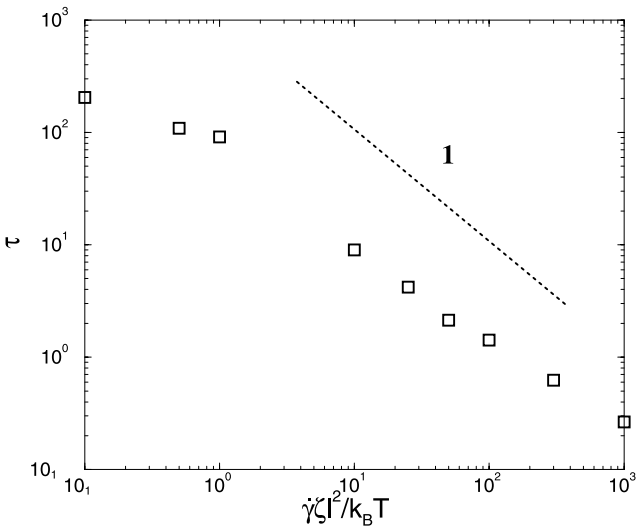

Fig. 5. Period of rotation of the polymer under simple shear flow as a function of shear rate.

in the zero shear rate limit. This explains the large error bars for material function data at extremely low shear rates.

3.2. Rheological quantities

We extracted the stress tensor $\boldsymbol{\pi}$ from the position vectors of the polymer, following the procedure detailed in P–M. The viscosity η, first normal stress coefficient, Ψ_1, and second normal stress coefficient, Ψ_2, can be calculated from the following equations.

$$\boldsymbol{\pi}_{yx} = -\eta\dot{\gamma}, \qquad \boldsymbol{\pi}_{xx} - \boldsymbol{\pi}_{yy} = -\Psi_1\dot{\gamma}^2, \qquad \boldsymbol{\pi}_{yy} - \boldsymbol{\pi}_{zz} = -\Psi_2\dot{\gamma}^2. \tag{12}$$

The material functions of the polymer chain under shear are found to have the following properties. The viscosity and the first normal stress coefficient both decrease as the shear rate increases, which is the signature of shear-thinning. The second normal stress coefficient is slightly negative. Our results for long polymer chains ($N = 60$) are shown in Fig. 6. They are qualitatively consistent with the behavior of material functions found by experiments and by P–M's previous simulations.

4. Results for elongational flow

For elongational flow, we are principally interested in the critical strain rate ε_c of the coil-stretch transition. This has been observed by experiments [6,11,15] and in some simulations [29], with and without including HI. Our results are summarized in Figs. 7–10. We have plotted R_g^2 as a function of strain rate in Fig. 7. The orientational order parameter, S, for the system, is defined as the ensemble-averaged value of the single bond order parameter S_i for bond i,

$$S_i = \tfrac{1}{2}(3\cos^2\theta - 1), \tag{13}$$

where θ_i is the angle between bond i and x axis. The coil state of the polymer corresponds to $S \sim 0.0$, while the fully stretched state corresponds to $S \sim 1.0$. The values of S for these two states are independent of the molecular weight N.

A plot of S as a function of the strain rate is shown in Fig. 8. Both Figs. 7 and 8 clearly show the existence of the coil-stretch transition. Although this does not appear to be a sharp transition, the slope of the inflection point of the $\log(R_g^2)$ vs $\log(\varepsilon)$ curve increases with increasing chain length, as shown in Fig. 9. This indicates a first order transition in the thermodynamic limit. We define the transition strain rate ε_c as the value of the strain rate at which the order parameter falls to $1/e$ (i.e. to 0.37). Using this definition of the transition strain rate, we have plotted ε_c as a function of molecular weight on a log–log scale in Fig. 10. A fit of the data points yields an exponent of $\beta = 1.4$, which is close to the values of around 1.5 found by the

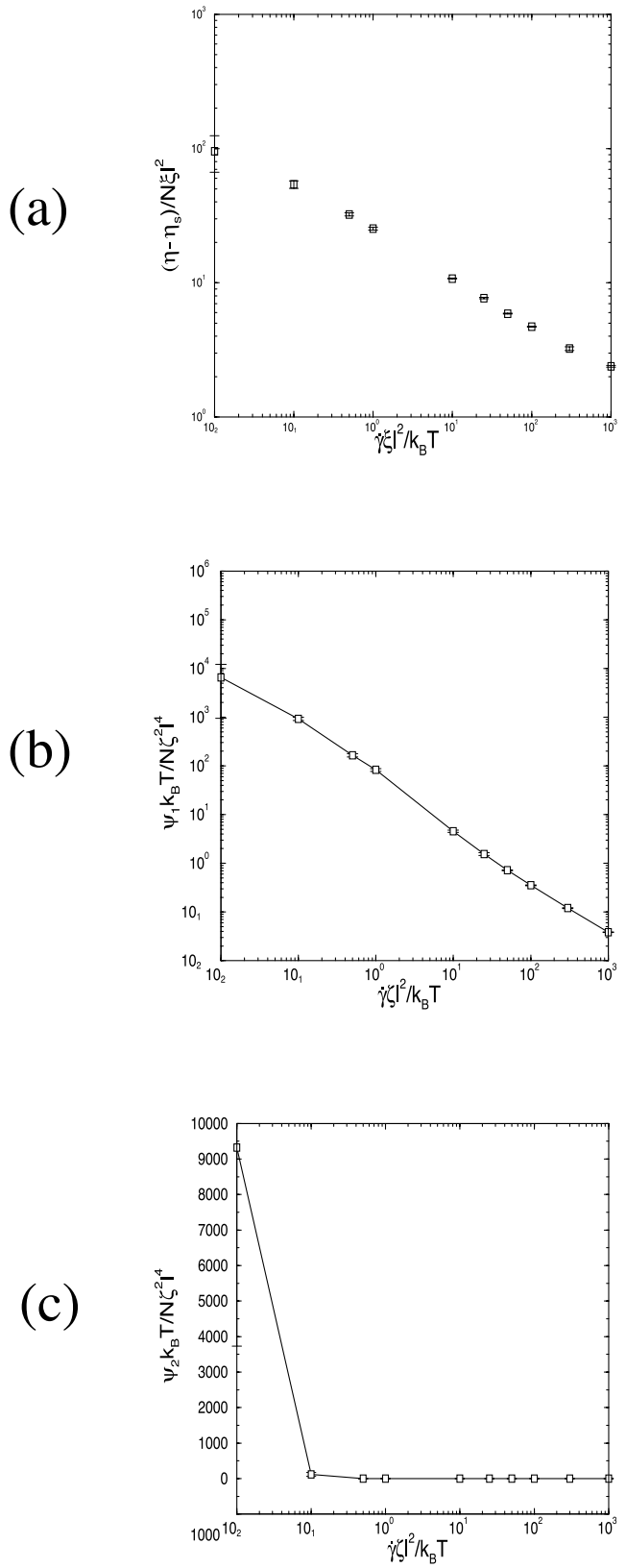

Fig. 6. Material functions of the polymer (a) reduced viscosity (η_s is the solvent viscosity), (b) first normal stress coefficient and (c) second normal stress coefficient as functions of shear rate.

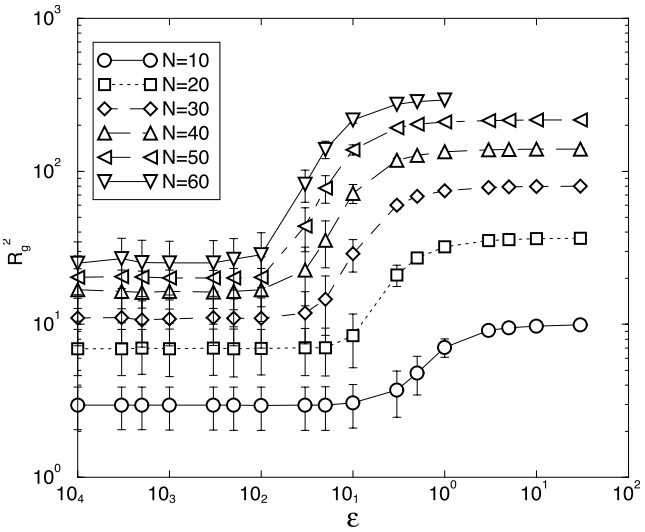

Fig. 7. Radius of gyration of the polymer under elongational flow as a function of strain rate, for different chain lengths, initial condition of the chains being a random coil.

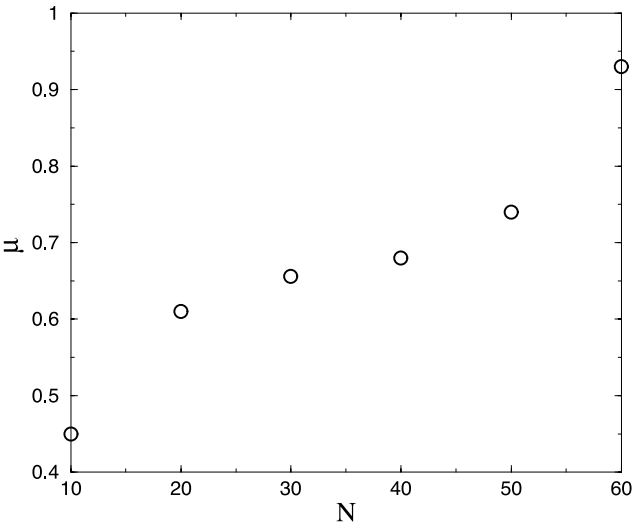

Fig. 9. Slopes (μ) of the $\log(R_g^2)$ vs $\log(\varepsilon)$ curves at the inflection point as function of chain length N (The values are obtained by the following procedure: the $\log(R_g^2)$ curves in Fig. 6 are first fitted with a logistic function and the slopes are then calculated at the inflection point).

experiments of Odell and Keller [6], Manasveta and Hoagland [11] amongst others, and in simulation results found by Hernandez Cifre and de la Torre [16] and Neelov et al. [17] using different models.

5. Discussion and conclusion

We implemented a Brownian dynamics algorithm for the simulation of a bead-rod-chain model for a dilute polymer solution under pure shear and elongational flows. The bead-rod-chain model constrains the bond length, thereby preserving the crucial property of inextensibility of the chemical bond, while models with bond extensibility might fail to display shear-thinning at high shear rates. We showed that our simulation produced the correct shear-thinning behavior even at very high shear rates. The model also gave the correct behavioral properties for the first and second normal stress coefficients. All these results are in agreement with earlier simulations done by P–M [38]. In that work, the longest chain simulated had 20 beads, while the present paper gives results for simulations for a chain up to 60 beads. By simulating a longer chain, we hoped to overcome any small-size effects that might have manifested themselves in the results obtained in the previous paper. In particular, the decrease of D_{33} with increase in shear rate was again observed in our simulations, although the decrease in the value of D_{33} was much slower than that of D_{22}. We believe that a chain length of 60 beads is still not sufficiently long enough to overcome any pathological effects that might result from the chain being too small. A much longer chain length might be needed to obtain better results.

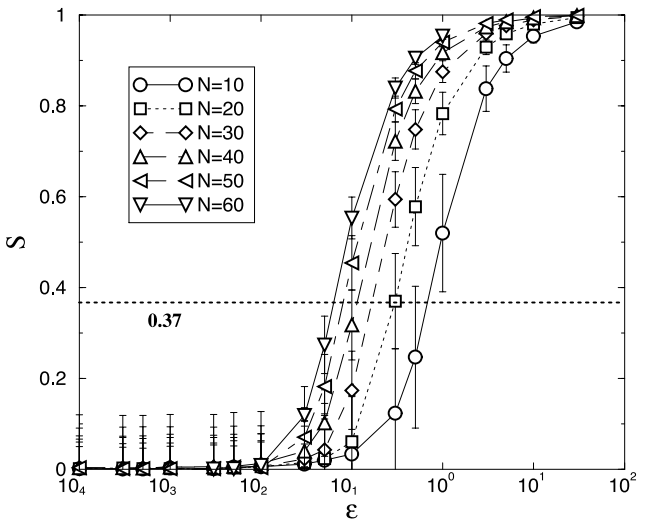

Fig. 8. Orientational order parameter of polymer plotted as a function of strain rate for different chain lengths.

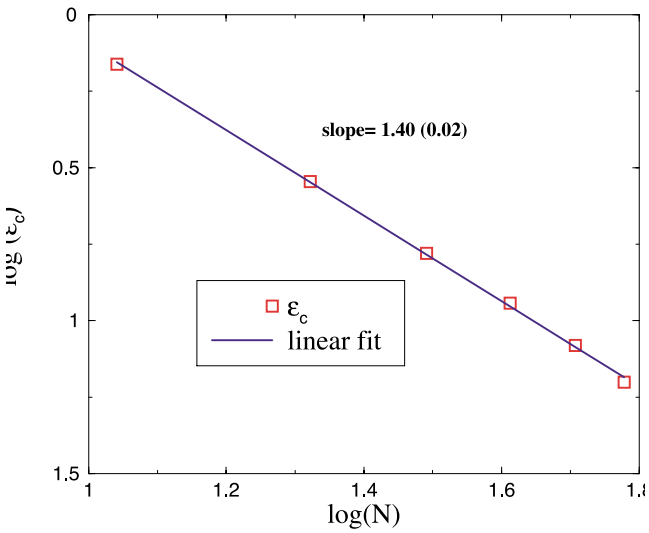

Fig. 10. Plot of critical elongational rate as a function of chain length.

We also simulated a dilute polymer solution in elongational flow. Our interest was in clarifying the nature (whether first-order or not) of the coil-stretch transition that is observed experimentally. Although this (Fig. 8) did not appear to be a sharp transition, the increase in slope at the inflection point of the log–log plot of R_g^2 vs ε with increase in chain length N (Fig. 9), points towards the occurrence of a first order transition in the thermodynamic limit. Instead of finding a sharp, abrupt transition, we found that the coil state migrated to the stretched state gradually as the flow rate increased. This result agrees with the theoretical prediction of a first-order transition by De Gennes [5] and observed in some simulations with HI, but is in disagreement with simulations done by Liu [26] and others. If hydrodynamic interaction between beads is suppressed, the transition is found to be of first order [30]. In the present work, hydrodynamics is represented only implicitly. The effects of explicit incorporation of hydrodynamics, by including all of the solvent particles, are not obvious and are to be explored in the future. We calculated the transition strain rate ε_c by keeping track of the order parameter, as described in the last section. We found an exponent of $\beta = 1.4$, for the decreasing dependence of ε_c on chain length, which is close to the experimental result [11].

The results of our simulations shown above underline the utility of the bead-rod-chain model in Brownian dynamics simulations of polymer fluids over a wide spectrum of flow rates, as we obtained correct results at very low flow rates, as well as at very high values. The disadvantage of this model, though, is that the computational time is higher than for some other simpler models such as the bead-spring model, as it uses the computationally expensive Shake algorithm [41] to constrain the bond length; it is hoped that further advances in computing power and algorithms will minimize this.

Acknowledgements

We would like to thank D. Petera and Prof. H. C. Öttinger for helpful discussions. Acknowledgment is made to the Materials Science Research and Engineering Center, University of Massachusetts, Amherst.

References

[1] Kotaka T, Suzuki H, Inagaki H. J Chem Phys 1966;45:2770.
[2] Huppler JD, Ashare E, Holmes LA. Trans Soc Rheol 1967;11:159.
[3] Vlassopoulos D, Schowalter WR. J Rheol 1995;38:1427.
[4] Tiu C, Moussa T, Carreau R. J Rheol Acta 1995;34:586.
[5] De Gennes PG. J Chem Phys 1974;60:5030.
[6] Odell JA, Keller A. J Polym Sci: Part B: Polym Phys 1986;24:1889.
[7] Keller A, Odell JA. Colloid Polym Sci 1985;263:181.
[8] Cathey CA, Fuller GG. J Non-Newtonian Fluid Mech 1990;34:63.
[9] Narh KA, Odell JA, Keller A. J Polym Sci, Polym Phys Ed 1992;30:335.
[10] Farrell CJ, Keller A, Miles MJ, Pope DP. Polymer 1980;21:1292.
[11] Menasveta MJ, Hoagland DA. Macromolecules 1992;25:7060.
[12] Brestkin YV, Saddikov IS, Agranova SA, Baranov VG, Frenkel S. Polym Bull 1986;15:147.
[13] Atkins EDT, Attwool PT, Miles MJ. Bristol Conference on Macromolecular Flexibility and Behaviour in Solution. Bristol, UK; 1986.
[14] Link A, Springer J. Macromolecules 1993;26:464.
[15] Perkins TT, Smith DE, Chu S. Science 1997;276:2016.
[16] Hernandez Cifre JG, de la Torre JG. J Rheol 1999;43:339.
[17] Neelov IM, Adolf DB, Lyulin AV, Davies GR. J Chem Phys 2002;117:4030.
[18] Rouse PE. J Chem Phys 1953;21:1272.
[19] Kirkwood JG, Riseman J. J Chem Phys 1948;16:565.
[20] Zimm BH. J Chem Phys 1956;24:269.
[21] Fixman M. J Chem Phys 1965;42:3831.
[22] Pyun CW, Fixman M. J Chem Phys 1965;42:3838.
[23] Pyun CW, Fixman M. J Chem Phys 1966;44:2107.
[24] Fixman M. J Chem Phys 1966;45:785.
[25] Fixman M. J Chem Phys 1966;45:793.
[26] Liu TW. J Chem Phys 1989;90:5826.
[27] Doyle PS, Shaqfeh ESG, Gast AP. J Fluid Mech 1997;334:251.
[28] Jendrejack RM, Graha MD, de Pablo JJ. J Chem Phys 2000;113:1.
[29] Larson RG, Hu H, Smith DE, Chu S. J Rheol 1999;43:267.
[30] Dukovski I, Muthukumar M. J Chem Phys 2003;118:6648.
[31] Bird RB, Armstrong C, Hassager O. Dynamics of polymeric liquids. Fluid mechanics, vol. 1. New York: Wiley; 1977.
[32] Bird RB, Curtiss CF, Armstrong C, Hassager O. Dynamics of polymeric liquids, 2nd ed. Kinetic theory, vol. 2. New York: Wiley; 1987.
[33] Yamakawa H. Modern theory of polymer solutions. New York: Harper and Row; 1971.
[34] Öttinger HC. Stochastic processes in polymeric fluids. Berlin: Springer; 1996.
[35] Öttinger HC. Phys Rev E 1994;50:2696.
[36] Öttinger HC. J Chem Phys 1989;90:463.
[37] Xu Z, Kim S, de Pablo JJ. J Chem Phys 1994;101:5293.
[38] Petera D, Muthukumar M. J Chem Phys 1999;111:7614.
[39] Kröoger M, Alba-Perez M, Laso M, Öttinger HC. J Chem Phys 2000;113:4767.
[40] Agarwal US. J Chem Phys 2000;113:3397.
[41] Ryckaert JP, Ciccotti G, Berendsen HJC. J Comput Phys 1977;23:327.
[42] Aust C, Hess S, Kröger M. Macromolecules 2002;35:8621.